Geophysical Research Letters

RESEARCH LETTER
10.1029/2020GL088985

Key Points:
- Inner magnetosphere field-aligned electron fluxes and dispersive Alfvén waves are strongly enhanced during storms and substorms
- Field-aligned electron energy and energy fluxes are strongly correlated with dispersive Alfvén wave energy densities and Poynting fluxes
- Oxygen ion outflows show strong correlations with field-aligned electron precipitation and dispersive Alfvén waves

Correspondence to:
A. J. Hull,
ahull@berkeley.edu

Citation:
Hull, A. J., Chaston, C. C., Bonnell, J. W., Damiano, P. A., Wygant, J. R., & Reeves, G. D. (2020). Correlations between dispersive Alfvén wave activity, electron energization, and ion outflow in the inner magnetosphere. *Geophysical Research Letters*, *47*, e2020GL088985. https://doi.org/10.1029/2020GL088985

Received 22 MAY 2020
Accepted 11 AUG 2020
Accepted article online 21 AUG 2020

Correlations Between Dispersive Alfvén Wave Activity, Electron Energization, and Ion Outflow in the Inner Magnetosphere

A. J. Hull[1], C. C. Chaston[1], J. W. Bonnell[1], P. A. Damiano[2], J. R. Wygant[3], and G. D. Reeves[4]

[1]Space Sciences Laboratory, University of California, Berkeley, CA, USA, [2]Geophysical Institute, University of Alaska Fairbanks, Fairbanks, AK, USA, [3]School of Physics and Astronomy, University of Minnesota, Twin Cities, Minneapolis, MN, USA, [4]Los Alamos National Laboratory, Los Alamos, NM, USA

Abstract Using measurements from the Van Allen Probes, we show that field-aligned fluxes of electrons energized by dispersive Alfvén waves (DAWs) are prominent in the inner magnetosphere during active conditions. These electrons have preferentially field-aligned anisotropies from 1.2 to >2 at energies ranging from tens of electron volts to several kiloelectron volts (keV), with largest values being coincident with magnetic field dipolarizations. Comparisons reveal that DAW energy densities and Poynting fluxes are strongly correlated with precipitating electron energies and energy fluxes and also O^+ ion outflow energies. These observations yield empirical inner magnetosphere relations between the DAW and electron inputs and the O^+ ion outflow response, providing important constraints for models. They also suggest that DAWs play an important role in enhancing field-aligned electron input into the ionosphere that facilitates the outflow and subsequent energization of O^+ ions in the wave fields into the inner magnetosphere.

Plain Language Summary We use satellite observations in the inner magnetosphere to study field-aligned electrons at kiloelectron volt energies and below. These electrons are invariably coincident with intense low-frequency electromagnetic waves called dispersive Alfvén waves (DAWs), which are prevalent during substorms and geomagnetic storms. Given that DAWs have parallel electric fields known to accelerate electrons, their simultaneous occurrences indicate that these waves are accelerating the electrons in the equatorial inner magnetosphere. Indicative of energization and heating in DAWs, the energies, number fluxes and energy fluxes of earthward-moving electrons are observed to increase with increasing DAW Poynting fluxes and energy densities. Given the ability of electron precipitation and DAWs to drive and produce energized ion outflow, we also tested for and demonstrated that oxygen ion outflow energies are strongly correlated with the electron and wave energy fluxes. Least squares fits yielded empirical relationships between the DAW, electron, and oxygen ion outflow characteristics, providing important constraints for models of plasma transport in the magnetospheric-ionospheric system. Owing to their persistent occurrence during active conditions and field-aligned sense, these wave energized electrons are expected to affect the growth and spatial distribution of other waves known to impact inner magnetosphere source and loss processes.

1. Introduction

Observations indicate that intense broadband Alfvénic fluctuations are prevalent in the active inner magnetosphere (e.g., Chaston, Bonnell, Kletzing, et al., 2015; Hull et al., 2019), with energy densities that are most intense during storms. Having wavelengths transverse to the magnetic field that extend below the ion gyroradius, these waves are dispersive in nature and are in the kinetic Alfvén wave regime. Though short across, these waves have wavelengths that are globally extended along the magnetic field and have waveforms that often exhibit interference signatures due to ionospheric reflection, which at times have characteristics of field line resonances or kinetic Alfvén eigenmodes of the geomagnetic field (Chaston et al., 2014). Owing to their global field line nature and often ionospheric connection, these waves are more accurately referred to as dispersive Alfvén waves (DAWs).

Alfvén waves play an important role in coupling the magnetosphere to the ionosphere via field-aligned currents, which act as conduits for plasma and wave energy flow and exchange between these disparate regions. At dispersive scales, Alfvénic fluctuations have an electric field component parallel to the background magnetic field. The time-variable currents associated with these fields can dissipate their energy into field-aligned electron heating and acceleration within the inner magnetosphere and all along the field line into the ionosphere (e.g., Chaston, 2006; Damiano et al., 2018; Hull et al., 2016). The resulting enhanced fluxes of precipitating electrons can drive multiscale Alfvénic aurora (Chaston et al., 2011; Wygant et al., 2000) and ion outflow from the ionosphere into the magnetosphere (Strangeway et al., 2005). Such energetic ion outflow can result from the synergistic action of DAW-enhanced "soft" electron precipitation combined with acceleration across thin transverse scales of DAWs with sufficiently large perpendicular electric fields. There is mounting evidence suggesting the importance of DAWs in the production of energized O^+ ion outflow into the magnetosphere (e.g., Chaston, Bonnell, Kletzing, et al., 2015; Chaston, Bonnell, Wygant, et al., 2015; Chaston et al., 2016). Associations between DAWs and ion outflow and field-aligned electrons are ubiquitous and have been observed in the dayside cusp region (Chaston et al., 2005), nightside plasma sheet boundary layer (Chaston et al., 2004; Wygant et al., 2002), in fast flows in the magnetotail (Chaston et al., 2012), and in the inner magnetosphere (Chaston et al., 2014; Malaspina et al., 2015), particularly during geomagnetic storms (Chaston, Bonnell, Kletzing, et al., 2015; Moya et al., 2015). In the inner magnetosphere intense DAWs have been observed coincident with energized field-aligned counterstreaming electrons (at a few keV energies and below) and ion outflow approaching tens of kiloelectron volts (e.g., Chaston, Bonnell, Wygant, et al., 2015; Hull et al., 2019). Correspondences between earthward Alfvénic Poynting fluxes and O^+ outflow deep in the inner magnetosphere have been observed (Gkioulidou et al., 2019). Correlations between DAW energy densities and outflowing O^+ energies and energy densities have also been reported (Hull et al., 2019). Using particle tracings, Chaston et al. (2016) demonstrated that the action of nonadiabatic particle motion in the thin fields of DAW field line resonance structure can explain the O^+ outflow energies observed in the equatorial inner magnetosphere. While these prior studies have provided evidence of the connections between DAWs, field-aligned electrons, and ionospheric O^+ outflow, important details of those relationships remain obscure.

This paper addresses the properties of $\lesssim$1 keV field-aligned electrons in the inner magnetosphere, their relationship to the energy content of DAWs and O^+ outflow, and how these electrons depend on the magnetospheric activity measures *AE* and *Sym-H*. Through detailed analysis of case and statistical data from the Van Allen Probes mission, we show that fluxes of field-aligned electrons are strongly enhanced in the inner magnetosphere during active geomagnetic conditions. We show for the first time that characteristic energies and energy fluxes of earthward-directed field-aligned electrons are strongly correlated with DAW energy densities and Poynting fluxes in the inner magnetosphere. We also show for the first time that outflowing ionospheric O^+ energies are strongly correlated with the downgoing field-aligned electron characteristic energies and energy fluxes and DAW Poynting fluxes. These correlated data are used to quantify empirical scaling relations between the DAW and electron inputs and the O^+ ion outflow energy response.

2. Results

2.1. Case Study

Figure 1 shows plasma and field data from the Van Allen Probes (denoted SC-A and SC-B) during an intense storm that commenced on 28 June 2013. This event was reported in an earlier study, which was focused on relationships between DAWs and ion outflow and energy densities (Hull et al., 2019). Here, we examine spatial and temporal interconnections between DAW activity and electrons in the inner magnetosphere. This storm has a minimum *Sym-H* value of −111 nT and is associated with *AE* peaking at 1,500 nT (2,400 nT) during the main (recovery) phase (see Figures 1a and 1b). Figure 1 shows roughly 2.5 orbits of data from SC-A and SC-B that span the main to early recovery phases of the storm indicated by the red and green bars at the top of Figure 1c. SC-B trails SC-A by roughly 3 hr and with apogee in the premidnight sector (see *L* values and magnetic local time [MLT] in Figures 1s and 1t).

Both spacecraft traverse the plasma sheet multiple times in the focus interval. Omnidirectional electron energy spectra from the Helium Oxygen Proton Electron (HOPE) instrument (Funsten et al., 2013) are shown in Figures 1c and 1k for SC-A and SC-B, respectively. The plasma sheet electrons correspond to the intense (red) energy flux signatures from a few to tens of keV energies in Figures 1c and 1k. From spacecraft

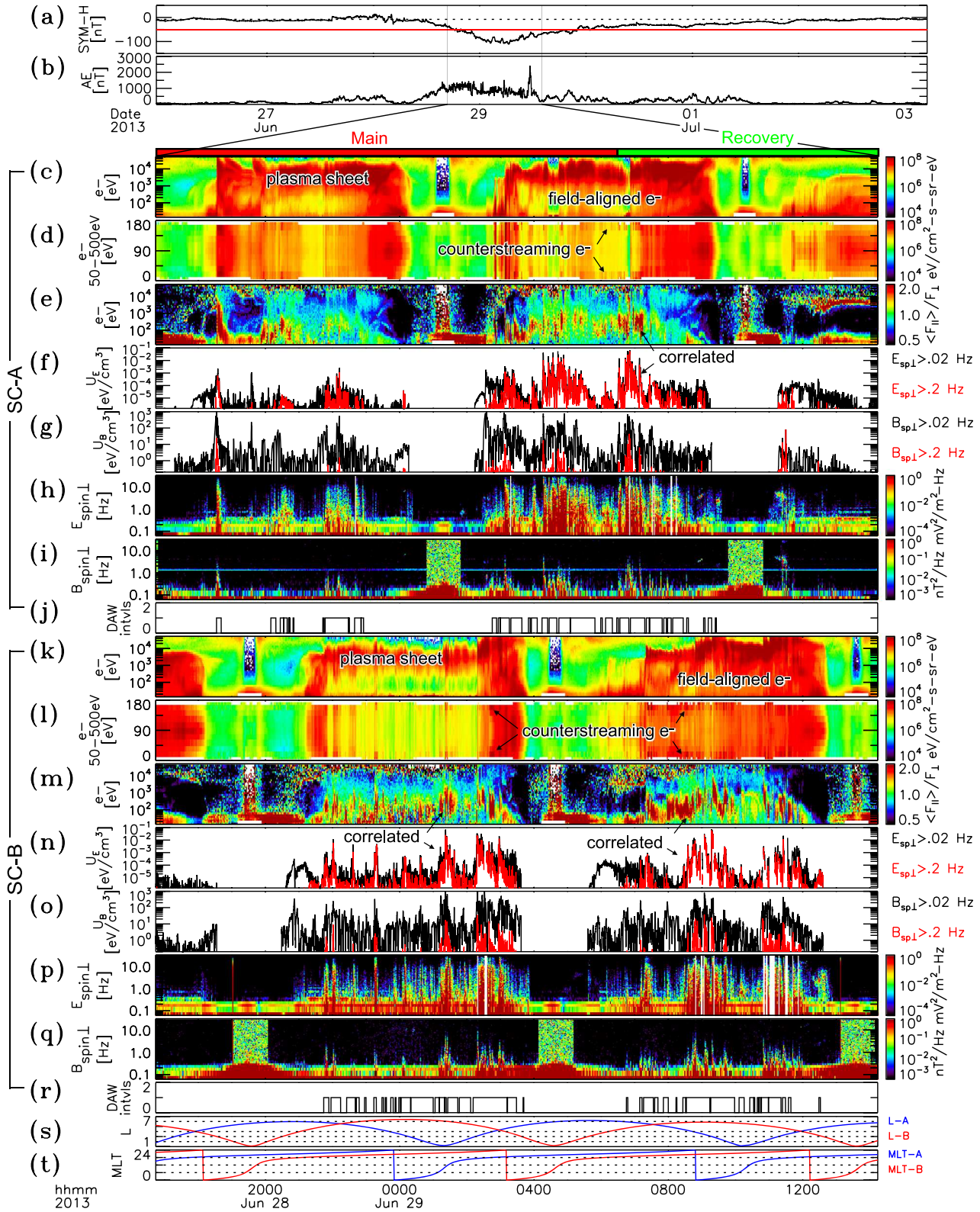

Figure 1. Van Allen Probes SC-A and SC-B data for the 28 June 2013 storm. Shown are (a) *Sym-H* and (b) the *AE* index. Zoomed in view of (c, k) electron energy flux energy spectra, (d, l) energy flux pitch angle spectra of 50–500 eV electrons, (e, m) electron anisotropy spectra, (f, n) electric and (g, o) magnetic field energy densities, (h, p) electric and (i, q) magnetic field power spectral densities, and (j, r) identified DAW intervals for SC-A (c–j) and SC-B (k–r). Also shown are (s) *L* and (t) MLT values for SC-A (blue) and SC-B (red).

to spacecraft and orbit to orbit, this population varies considerably, with multiple energy flux intensifications occurring during the storm, associated with injections of hotter plasma into the inner magnetosphere. Lower-energy electrons spanning broad energies from a few keV and below are also observed throughout the plasma sheet region. These have a preferential magnetic field-aligned sense and usually appear in the inner magnetosphere with counterstreaming signatures as indicated in the pitch angle spectra of 50–500 eV electrons shown in Figures 1d and 1l. The field-aligned nature and energy span of these electrons are discernible from the anisotropy spectra displayed in Figures 1e and 1m. The anisotropy is defined as the ratio of field-aligned (average of 0–30° and 150–180° pitch angle ranges) and perpendicular (75–105°) electron energy fluxes. The anisotropy spectra reveal that these electrons have preferential parallel anisotropies ranging from 1.2 to >2 (yellow to red) in the interval. This population is easily distinguished from the plasma sheet electrons, which are isotropic (green) near apogee or have preferential perpendicular anisotropy (blue to black) at lower L-shell. The field-aligned electron maximum energies in the anisotropy spectra also have variations that are correlated with the electric and magnetic field energy densities of intense long-duration bursts of low-frequency waves identified as DAWs in the study by Hull et al. (2019). The electric and magnetic field energy densities are displayed in Figures 1f and 1g for SC-A and Figures 1n and 1o for SC-B. These were derived from electric and magnetic fields measured from the Electric Field and Waves (EFW) instrument (Wygant et al., 2013) and the Electric and Magnetic Field Instrument Suite and Integrated Science (EMFISIS) instrument (Kletzing et al., 2013), respectively. Following Hull et al. (2019), the wave energy densities are shown in two frequency ranges, with black spanning both the nondispersive and DAW frequency ranges (0.02 to 16 Hz) and red the dispersive range (0.2 to 32 Hz). Electric and magnetic field power spectral densities are shown in Figures 1h and 1i for SC-A and Figures 1p and 1q for SC-B, respectively. Intervals attributed to DAWs are indicated by the unity values in Figures 1j and 1r for SC-A and SC-B, respectively. These intervals were determined using an automatic procedure that detects Doppler shifted DAWs in the frequency range from $0.01 < f_{SC} < 20$ Hz via the $E_{\perp}/B_{\perp}$ ratio characteristics (Chaston, Bonnell, Kletzing, et al., 2015).

To further examine relationships, Figure 2 shows electron and wave data from SC-B in a zoomed in interval encompassing one of the plasma sheet transects in Figure 1. Field-aligned electrons, at a few keV and below, appear throughout the interval indicated by the yellow to red enhancements in electron anisotropy in Figure 2c. The highest energies occur in association with magnetic field dipolarizations indicated by sharp increases in the inclination angle ($\theta_{inc} \equiv \tan^{-1}[B_{GSMz}/(B^2_{GSMx} + B^2_{GSMy})^{1/2}]$) shown in Figure 2k. Figures 2d–2f, respectively, show the characteristic energy (defined as the energy flux divided by the number flux), number flux, and energy flux of the low-energy, wave accelerated electrons at pitch angles $\alpha < 90°$ (i.e., propagate downward toward the Northern Hemisphere). These quantities were computed from moments of the pitch angle distribution over the electron energies associated with energy flux anisotropies >1.2. For context, the characteristic energy is indicated by the black curve in Figure 2c.

To compare, Figures 2g and 2h present electric and magnetic field energy densities in the two frequency bands, and Figure 2i gives the parallel Poynting flux. The unity values in Figure 2j verify that the enhanced wave activity in the interval is due to DAWs. Comparisons suggest that the variations in the electron quantities (particularly the characteristic energy and energy flux) are strongly correlated with the DAW electric and magnetic field energy densities and the parallel Poynting flux.

To quantify relationships, Figures 3a and 3b show the electric field energy densities U_E of Alfvén waves at dispersive scales (at frequencies above 0.2 Hz) as function of the characteristic energies E_e^{ch} and energy fluxes $\mathcal{E}_e$ of the downgoing field-aligned electrons sampled by SC-B in all identified DAW intervals shown in Figure 1r. Strong positive correlations are apparent, with coefficients of $r = 0.54$ and $r = 0.62$ found for log space data quantities shown in Figures 3a and 3b, respectively. A log space linear regression analysis, with errors in both the dependent and independent variables (Press et al., 1996), was applied to data averaged in equally spaced $\log_{10}(U_E)$ bins (red dots). The log space fits to $\log_{10}(y) = m\log_{10}(x) + b$, with m being the slope and b the intercept, take the form of a power law $y = cx^m$ in "true" space, where $c = 10^b$. Thus, the analysis yielded the power law relations $E_e^{ch} = 10^{4.1\pm0.3}U_E^{0.36\pm0.10}$ and $\mathcal{E}_e = 10^{4.1\pm0.3}U_E^{0.53\pm0.10}$, respectively. A strong positive correlation ($r = 0.63$) is also shown in Figure 3c, which compares field-aligned electron energy fluxes with parallel Poynting fluxes $S_{\parallel}$ of Alfvén waves at dispersive scales (frequencies above 0.2 Hz). Only $S_{\parallel}$ associated with magnetic fields above an estimated noise floor of 0.15 nT are shown. Regression analysis yielded the relation $\mathcal{E}_e = 10^{2.1\pm0.3}S_{\parallel}^{0.54\pm0.21}$. These empirical relationships are a quantification of electron acceleration via parallel electric fields in the DAWs present in the interval and noted in prior studies (e.g., Chaston, Bonnell, Wygant, et al., 2015).

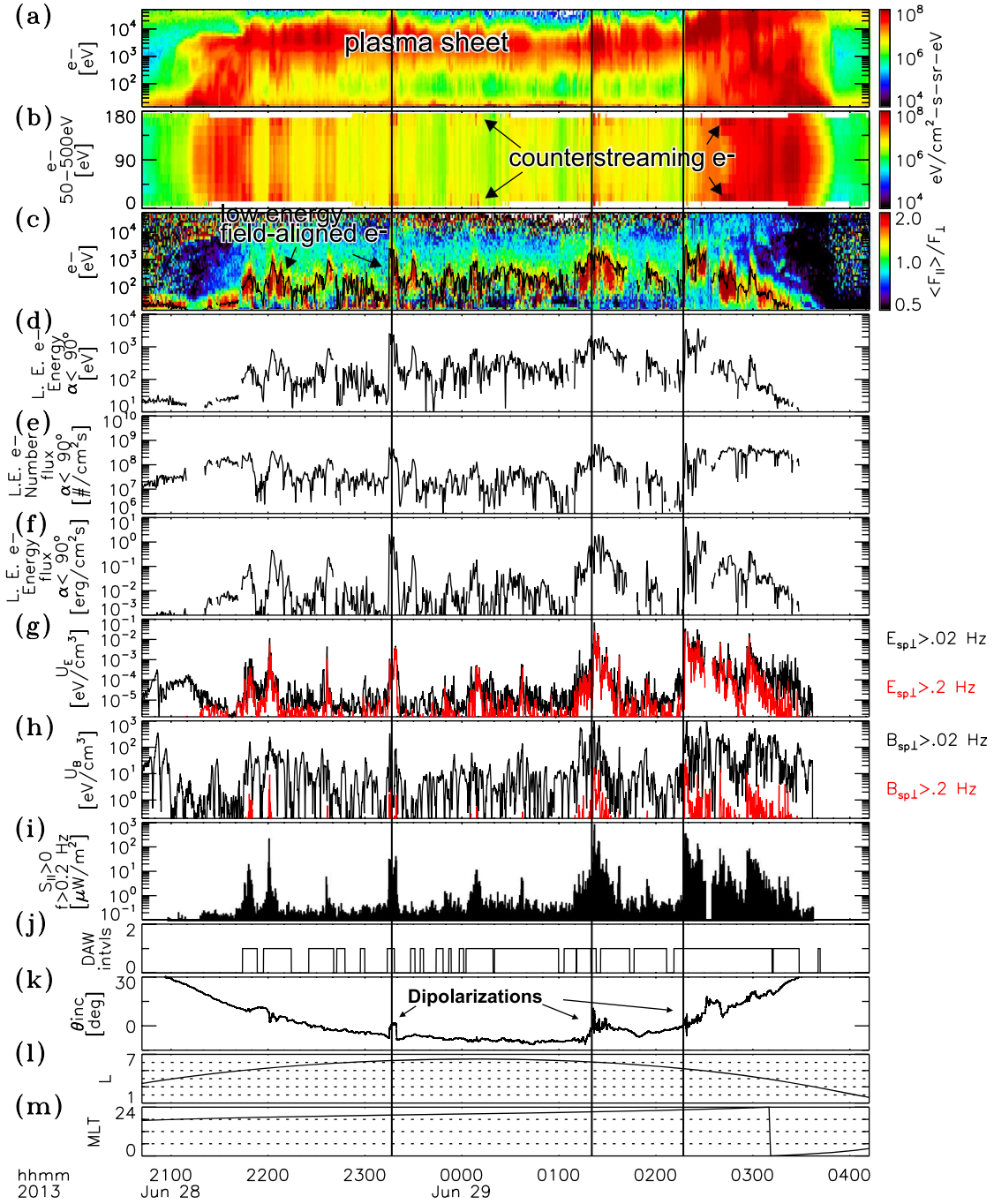

Figure 2. Data from SC-B in zoomed in interval. Shown are the (a) electron energy flux energy spectra, (b) energy flux pitch angle spectra of 50 to 500 eV electrons, (c) electron anisotropy spectra, the (d) characteristic energy, (e) number flux, (f) and energy flux of downgoing low-energy electrons, (g) electric and (h) magnetic field energy densities, (i) downgoing parallel Poynting flux, (j) identified DAW intervals,(k) magnetic field inclination angle, (l) L-shell, and (m) MLT. The black vertical lines indicate example magnetic field dipolarizations. The black curve in (c) is the low-energy electron characteristic energy.

To examine electron and ion relationships, Figures 3d and 3e show outflowing O^+ ion peak energies E_{O^+} versus field-aligned electron characteristic energies and energy fluxes, respectively. Both comparisons show strong correlations with coefficients of 0.63 and 0.57, respectively. Values for E_{O^+}, initially reported by Hull et al. (2019), are determined as the energy at the peak ratio between antiparallel ($150° \leq \alpha \leq 180°$) and perpendicular ($75° \leq \alpha \leq 105°$) O^+ flux spectra associated with an identified outflowing beam. A strong positive correlation ($r = 0.67$) between the outflowing O^+ peak energies and the DAW parallel Poynting

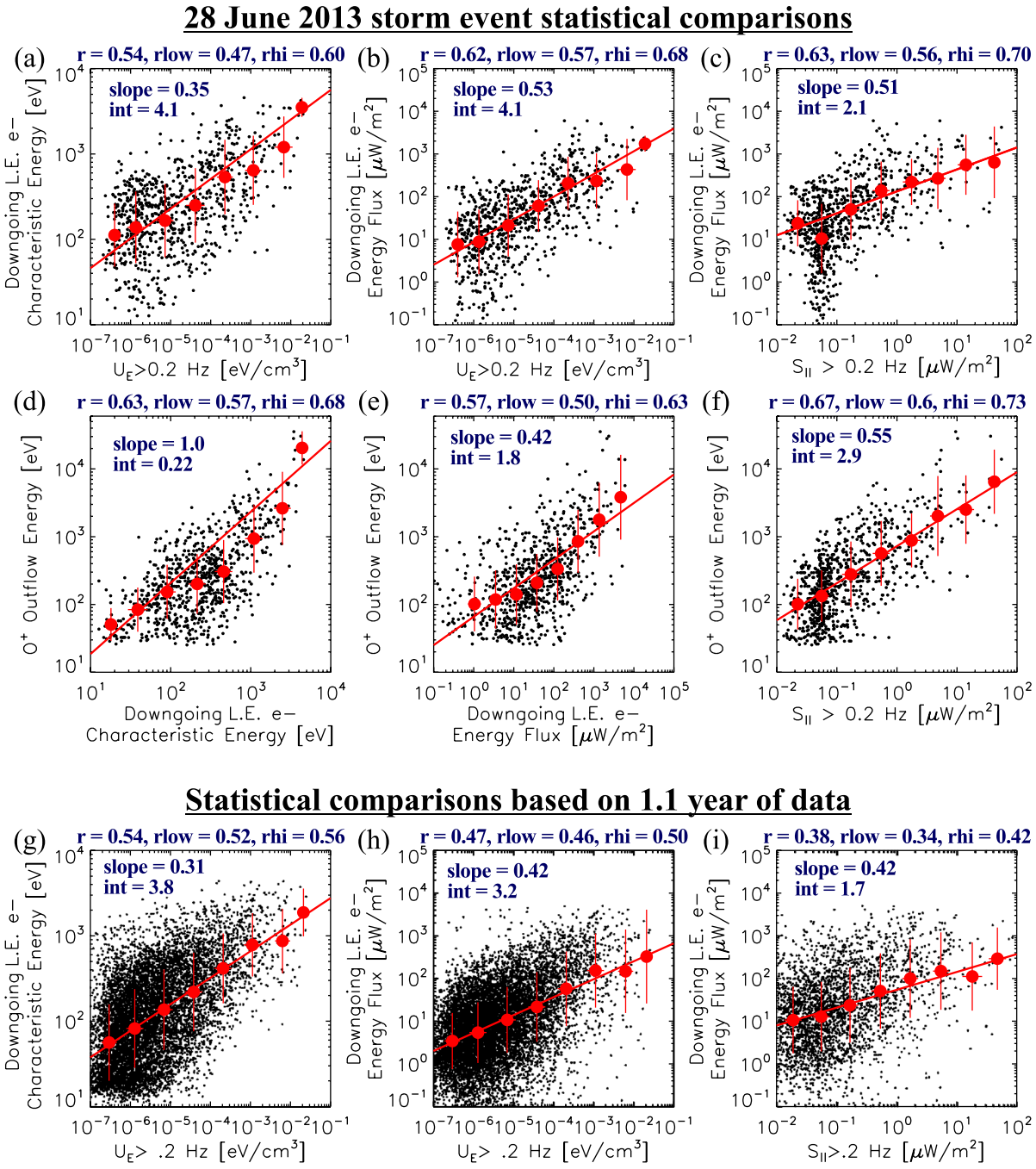

Figure 3. (a–f) Data from SC-B for identified DAW intervals in the 28 June 2013 storm interval in Figure 1. Compares U_E with downgoing DAW accelerated electron (a) characteristic energies and (b) energy fluxes and (c) DAW parallel Poynting fluxes with downgoing DAW accelerated electron energy fluxes. Compares O^+ outflow energy with downgoing DAW accelerated electron (d) characteristic energies and (e) energy fluxes and (f) DAW parallel Poynting fluxes, respectively. (g–i) SC-B data for identified DAW intervals spanning from 11 November 2012 to 31 December 2013. Compares U_E with downgoing DAW accelerated electron (g) characteristic energies and (h) energy fluxes and (i) DAW parallel Poynting fluxes with downgoing DAW accelerated electron energy fluxes. Red dots and bars in each plot show log space bin averages and standard deviations. The red solid lines show linear fits. Correlation coefficients and 99% confidence low and high limits are listed above each panel. Since the low and high confidence limits do not bound 0, the correlations shown are statistically significant.

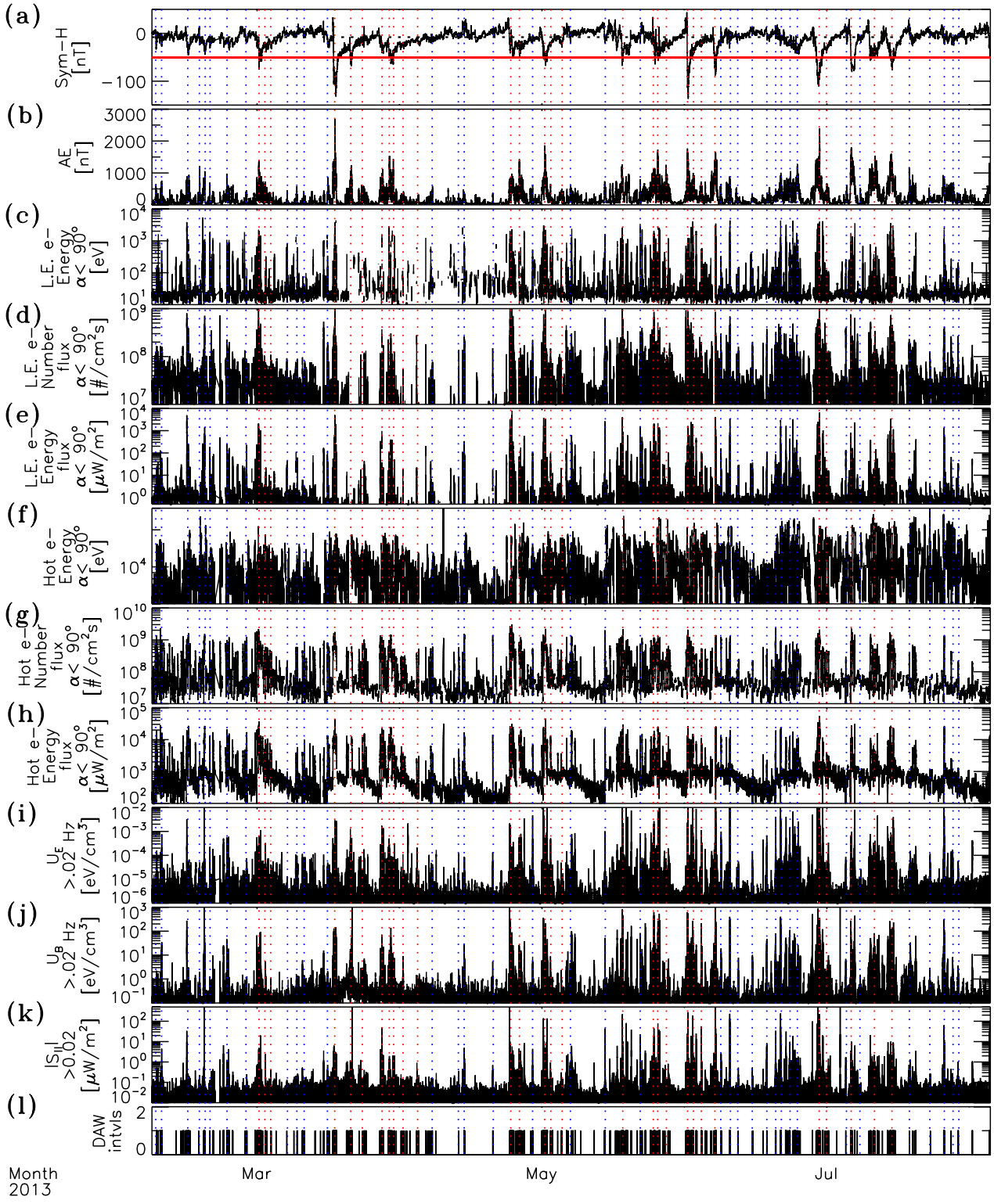

Figure 4. (a) *Sym-H*, (b) *AE* index, downgoing low-energy field-aligned electron (c) characteristic energy, (d) number flux, and (e) energy flux, downgoing hot electron (f) characteristic energy, (g) number flux, and (h) energy flux, energy densities of (i) electric and (j) magnetic fields above 0.02 Hz, (k) Poynting fluxes above 0.02 Hz, and (l) DAW intervals. The red horizontal line in (a) indicates the −50 nT storm *Sym-H* threshold, while the black dashed line gives the full year median value (−7 nT). Vertical dotted lines indicate select peaks in *AE* during nonstorm (blue) and storm (red) conditions.

fluxes is also demonstrated in Figure 3f. Regression analysis yielded the relations $E_{O^+} = 10^{0.22\pm0.51} E_e^{ch\,1.0\pm0.2}$, $E_{O^+} = 10^{1.8\pm0.2} \mathcal{E}_e^{0.42\pm0.08}$, and $E_{O^+} = 10^{2.9\pm0.1} S_{||}^{0.55\pm0.05}$ for data shown in Figures 3d–3f, respectively.

2.2. Statistical Correlations and Temporal Variations Over a Range of Conditions

To examine statistical correlations over a range of conditions, Figures 3g and 3h compare DAW accelerated downgoing electron energies and energy fluxes with the electric field energy densities at dispersive scales for all identified DAW intervals in 1 min data samples from SC-B spanning from 11 November 2012 to 31 December 2013. As shown below, the DAWs are characteristic of substorm and storm time conditions. The comparisons in Figures 3g and 3h reveal positive correlations with coefficients of 0.54 and 0.47, respectively. Regression analysis applied to bin-averaged data (red dots) shown in Figures 3g and 3h yielded the relations $E_e^{ch} = 10^{3.8\pm0.2} U_E^{0.31\pm0.05}$ and $\mathcal{E}_e = 10^{3.2\pm0.4} U_E^{0.42\pm0.07}$, respectively. Comparisons between field-aligned electron energy fluxes and DAW parallel Poynting fluxes in Figure 3i also reveal a relatively weaker, but statistically significant, correlation with a coefficient of $r = 0.38$ and 99% confidence interval of $r_{low} = 0.34$, $r_{hi} = 0.42$. Fits to the bin-averaged data yielded the relation $\mathcal{E}_e = 10^{1.7\pm0.2} S_{||}^{0.42\pm0.13}$. Within the errors, these results are consistent with the single event statistics presented in Figures 3a–3c, demonstrating the robustness of the empirical relations determined from DAW and electron observations over varied magnetospheric conditions.

To examine the long time behavior of field-aligned electrons in relation to DAWs and activity measures, Figure 4 shows roughly 6 months of data from SC-B sampled every minute from 6 February to 5 August 2013. This is the same time interval used in the study by Hull et al. (2019), who reported O^+ and Alfvén wave energy density correlations with *Sym-H* and the *AE* index. During this interval apogee precessed westward from ~2.5 to ~19.5 MLT, which spans the midnight and dusk sectors of the inner magnetosphere. This interval contains several storms and substorms, as indicated by *Sym-H* extending below −50 nT in Figure 4a and $AE > 300$ nT in Figure 4b, respectively. Figures 4c–4e show the characteristic energies, number fluxes, and energy fluxes of DAW energized field-aligned electrons moving toward Earth's northern ionosphere, respectively. These electrons occur at virtually all periods with $AE > 300$ nT, as evidenced by coincident sizable increases in their characteristic energies, number fluxes and energy fluxes. As a guide, vertical dotted lines are given in Figure 4 at peaks in $AE \gtrsim 300$ nT coincident with DAW activity (unity values in Figure 4l). The lines are color coded, with blue and red indicating nonstorm and storm (main to recovery) time conditions, respectively. The data reveal that DAW energized field-aligned electrons are a characteristic feature of the inner magnetosphere during substorm active periods. With the largest values occurring during magnetic storms, these electrons have downgoing energies ranging from tens of electron volts to a few kiloelectron volts and have number and energy fluxes extending to several #/cm^2 s and a few thousand μW/m^2, respectively (see Figures 4c–4e). Indicative of their energization mechanism, the enhanced field-aligned electrons are collocated with the electric and magnetic field energy densities and parallel Poynting fluxes carried by Alfvén waves, which are shown in Figures 4i–4k. The electric and magnetic field energy densities and Poynting fluxes associated with Alfvén waves at nondispersive to dispersive scale (e.g., above 0.02 Hz) also tend to have largest values at storm time substorms with peak values reaching $\gtrsim 10^{-2}$ eV/cm^3, $\gtrsim 10^3$ eV/cm^3, and $\gtrsim$500 μW/m^2, respectively. Hot plasma sheet electrons show similar but much stronger enhancements in the number and energy fluxes that are collocated with non–storm and storm time substorm active conditions (Figures 4f–4h). We attribute such enhancements to the injection of hotter and denser plasma sheet electrons to the inner magnetosphere.

3. Discussion

These empirical relations quantified from inner magnetosphere measurements for the first time indicate that the factors that impact ion outflow are operative therein. Though the power index values are not fully understood, these relations are consistent with the scenario where the O^+ ion outflow is controlled by the combined action of DAW energized electron precipitation and DAW transverse energization along the field (Chaston et al., 2016). Though analogous, these scaling relations differ from relations determined at much lower altitudes in the dayside auroral/cusp region by Strangeway et al. (2005) and Zheng et al. (2005). Both studies showed positive correlations between ion outflow fluxes and very low frequency/quasistatic (denoted as direct current, DC) Poynting fluxes, but ion and electron energy fluxes showed weak to no correlation. Though ion fluxes were not addressed here, the strong positive correlations between O^+ energy and both low-energy electron energy and DAW Poynting fluxes may be indicative of correlations with O^+ fluxes

in the limit of nearly constant beam density. Our comparisons differ in that the measurements are from the nightside, and we compare low-energy field-aligned electron contributions separated from more energetic components, Alfvén wave quantities at dispersive scale, and O^+ ion energies instead of ion fluxes, which may explain trend differences. Also, the correlation between O^+ energy and low-energy electron energy differs from results of Seo et al. (1997), who showed upflowing ion velocities (hence energies) in the topside ionosphere are anticorrelated with soft electron precipitation energies. Our results are not necessarily contradictory since the O^+ ion energies include the additional effects of substantial transverse ion energization combined with magnetic mirroring and thus are not expected to have the same behavior.

Finally, we note that short-duration time domain structures (TDS) (Mozer et al., 2015) are often embedded at higher frequencies within the lower-frequency DAWs (Chaston, Bonnell, Kletzing, et al., 2015). The relative role of these modes in driving parallel electron acceleration and heating has not been established. However, while field-aligned electron distributions are always observed in DAWs, TDS are not. Moreover, kinetic simulations demonstrate that DAW activity alone can reproduce observed energies and distribution features (Damiano et al., 2018). A description of electron acceleration processes in TDS is provided by Vasko et al. (2017).

4. Summary and Conclusions

We examined the properties of field-aligned electrons and their relation to DAW Poynting fluxes and energy densities, and O^+ outflow in the inner magnetosphere. We showed that field-aligned fluxes of electrons consistent with DAW energization are prominent in the inner magnetosphere during active conditions, occurring at virtually every storm and substorm. These electrons are associated with enhanced DAW Poynting fluxes and energy densities and are accompanied by injections of enhanced fluxes of hot plasma sheet electrons. During storm time periods, correlated energized electrons and DAW activity persist for large fractions of a day over a large L-shell and azimuthal extent of the plasma sheet. These electrons have preferentially field-aligned flux anisotropies from 1.2 to >2 at keV energies and below, with largest energies being coincident with magnetic field dipolarizations. The downgoing low-energy field-aligned electron energies and energy fluxes were shown, for the first time, to be strongly positively correlated with DAW electric field energy densities and parallel Poynting fluxes in the inner magnetosphere. Peak O^+ outflow energies were also shown to be strongly correlated with DAW Poynting fluxes and downgoing field-aligned electron characteristic energies and energy fluxes. Regression analysis to single storm case and 12 month statistical data yielded quantitatively consistent empirical inner magnetosphere relations between the DAW and electron inputs and the O^+ ion outflow energy response, which can be used to test magnetosphere-ionosphere transport models.

These results in combination with other reports (e.g., Chaston, Bonnell, Kletzing, et al., 2015; Chaston, Bonnell, Wygant, et al., 2015; Chaston et al., 2016; Damiano et al., 2018; Hull et al., 2019) highlight the important role played by DAWs in coupling the ionosphere to the magnetosphere via global field-aligned energy transport and dissipation processes with important ramifications to magnetospheric structure and dynamics. The results suggest that such processes are initiated and driven by injections in the equatorial magnetosphere. Owing to their persistent global nature in L-shell, azimuth, and along the magnetic field during active conditions, the DAWs continuously energize electrons into the ionosphere, which facilitates O^+ upwelling from the topside ionosphere while also driving multiscale Alfvénic aurora. Subsequent nonadiabatic transverse acceleration in DAW electric fields combined with the magnetic mirror force yield energized ion outflow in the inner magnetosphere that contributes to plasma sheet and ring current populations and strongly impact their structure and dynamics. The pervasive enhancement of electrons up to several keV by DAWs during active magnetic conditions almost certainly impacts the growth and distribution of other wave modes, such as oblique whistlers (e.g., Artemyev et al., 2016) known to impact outer radiation belt sources and losses. While not quantified in this study, the extent to which DAWs and associated energized electrons (and also ion outflow) impact the occurrence and spatial distribution of other attendant modes is an important outstanding problem that will require additional statistical studies, which we leave for future work.

Data Availability Statement

Data used are publicly available at the following repositories: HOPE (https://rbsp-ect.lanl.gov/), EMFISIS (https://emfisis.physics.uiowa.edu/), and EFW (http://www.space.umn.edu/rbspefw-data/).

Acknowledgments
A. J. Hull and/or C. C. Chaston received support from Grants 80NSSC18K0835, NNX17AD36G, NNX17A155G, NNX16AG69G, NSF1602941, and 80NSSC19K0081 sub PO36751. P. A. Damiano received support from Grants NSF1832207 and 80NSSC18K0835. Van Allen Probes funding is provided under NASA prime Contract NAS5-01072; including the EFW investigation, the EMFISIS investigation under JHU/APL Contract 921647, and RBSP-ECT JHU/APL under Contract 967399. We acknowledge use of the SPEDAS software to download and analyze data (Angelopoulos et al., 2019).

References

Angelopoulos, V., Cruce, P., Drozdov, A., Grimes, E. W., Hatzigeorgiu, N., King, D. A., & Schroeder, P. (2019). The Space Physics Environment Data Analysis System (SPEDAS). *Space Science Reviews*, *215*(1), 9. https://doi.org/10.1007/s11214-018-0576-4

Artemyev, A., Agapitov, O., Mourenas, D., Krasnoselskikh, V., Shastun, V., & Mozer, F. (2016). Oblique whistler-mode waves in the Earth's inner magnetosphere: Energy distribution, origins, and role in radiation belt dynamics. *Space Science Reviews*, *200*(1-4), 261–355. https://doi.org/10.1007/s11214-016-0252-5

Chaston, C. C. (2006). ULF waves and auroral electrons. In K. Takahashi, P. Chi, R. E. Denton, & R. L. Lysak (Eds.), *Magnetospheric ULF waves* (vol. 169, pp. 229–257).

Chaston, C. C., Bonnell, J. W., Carlson, C. W., McFadden, J. P., Ergun, R. E., Strangeway, R. J., & Lund, E. J. (2004). Auroral ion acceleration in dispersive Alfvén waves. *Journal of Geophysical Research*, *109*, A04205. https://doi.org/10.1029/2003JA010053

Chaston, C. C., Bonnell, J. W., Clausen, L., & Angelopoulos, V. (2012). Energy transport by kinetic-scale electromagnetic waves in fast plasma sheet flows. *Journal of Geophysical Research*, *117*, A09202. https://doi.org/10.1029/2012JA017863

Chaston, C. C., Bonnell, J. W., Kletzing, C. A., Hospodarsky, G. B., Wygant, J. R., & Smith, C. W. (2015). Broadband low-frequency electromagnetic waves in the inner magnetosphere. *Journal of Geophysical Research: Space Physics*, *120*, 8603–8615. https://doi.org/10.1002/2015JA021690

Chaston, C. C., Bonnell, J. W., Reeves, G. D., & Skoug, R. M. (2016). Driving ionospheric outflows and magnetospheric O^+ energy density with Alfvén waves. *Geophysical Research Letters*, *43*, 4825–4833. https://doi.org/10.1002/2016GL069008

Chaston, C. C., Bonnell, J. W., Wygant, J. R., Kletzing, C. A., Reeves, G. D., Gerrard, A., & Smith, C. W. (2015). Exteme ionospheric ion energization and electron heating in Alfvén waves in the storm time inner magnetosphere. *Geophysical Research Letters*, *42*, 10,531–10,540. https://doi.org/10.1002/2015GL066674

Chaston, C. C., Bonnell, J. W., Wygant, J. R., Mozer, F., Bale, S. D., Kersten, K., & MacDonald, E. A. (2014). Observations of kinetic scale field line resonances. *Geophysical Research Letters*, *41*, 209–215. https://doi.org/10.1002/2013GL058507

Chaston, C. C., Peticolas, L. M., Carlson, C. W., McFadden, J. P., Mozer, F., Wilber, M., & Balogh, A. (2005). Energy deposition by Alfvén waves into the dayside auroral oval: Cluster and FAST observations. *Journal of Geophysical Research*, *110*, 2211. https://doi.org/10.1029/2004JA010483

Chaston, C. C., Seki, K., Sakanoi, T., Asamura, K., Hirahara, M., & Carlson, C. W. (2011). Cross-scale coupling in the auroral acceleration region. *Geophysical Research Letters*, *38*, 20101. https://doi.org/10.1029/2011GL049185

Damiano, P. A., Chaston, C. C., Hull, A. J., & Johnson, J. R. (2018). Electron distributions in kinetic scale field line resonances: A comparison of simulations and observations. *Geophysical Research Letters*, *45*, 5826–5835. https://doi.org/10.1029/2018GL077748

Funsten, H. O., Skoug, R. M., Guthrie, A. A., MacDonald, E. A., Baldonado, J. R., Harper, R. W., & Chen, J. (2013). Helium, Oxygen, Proton, and Electron (HOPE) mass spectrometer for the Radiation Belt Storm Probes mission. *Space Science Reviews*, *179*, 423–484. https://doi.org/10.1007/s11214-013-9968-7

Gkioulidou, M., Ohtani, S., Ukhorskiy, A. Y., Mitchell, D. G., Takahashi, K., Spence, H. E., & Barnes, R. J. (2019). Low-energy (<keV) O^+ ion outflow directly into the inner magnetosphere: Van Allen Probes observations. *Journal of Geophysical Research: Space Physics*, *124*, 405–419. https://doi.org/10.1029/2018JA025862

Hull, A. J., Chaston, C. C., Bonnell, J. W., Wygant, J. R., Kletzing, C. A., Reeves, G. D., & Gerrard, A. (2019). Dispersive Alfvén wave control of O^+ ion outflow and energy densities in the inner magnetosphere. *Geophysical Research Letters*, *46*, 8597–8606. https://doi.org/10.1029/2019GL083808

Hull, A. J., Chaston, C. C., Frey, H. U., Fillingim, M. O., Goldstein, M. L., Bonnell, J. W., & Mozer, F. S. (2016). The "Alfvénic" surge at substorm onset/expansion and the formation of "Inverted Vs" : Cluster and IMAGE observations. *Journal of Geophysical Research: Space Physics*, *121*, 3978–4004. https://doi.org/10.1002/2015JA022000

Kletzing, C. A., Kurth, W. S., Acuna, M., MacDowall, R. J., Torbert, R. B., Averkamp, T., & Tyler, J. (2013). The Electric and Magnetic Field Instrument Suite and Integrated Science (EMFISIS) on RBSP. *Space Science Reviews*, *179*, 127–181. https://doi.org/10.1007/s11214-013-9993-6

Malaspina, D. M., Wygant, J. R., Ergun, R. E., Reeves, G. D., Skoug, R. M., & Larsen, B. A. (2015). Electric field structures and waves at plasma boundaries in the inner magnetosphere. *Journal of Geophysical Research: Space Physics*, *120*, 4246–4263. https://doi.org/10.1002/2015JA021137

Moya, P. S., Pinto, V. A., Viñas, A. F., Sibeck, D. G., Kurth, W. S., Hospodarsky, G. B., & Wygant, J. R. (2015). Weak kinetic Alfvén waves turbulence during the 14 November 2012 geomagnetic storm: Van Allen Probes observations. *Journal of Geophysical Research: Space Physics*, *120*, 5504–5523. https://doi.org/10.1002/2014JA020281

Mozer, F. S., Agapitov, O. V., Artemyev, A., Drake, J. F., Krasnoselskikh, V., Lejosne, S., & Vasko, I. (2015). Time domain structures: What and where they are, what they do, and how they are made. *Geophysical Research Letters*, *42*, 3627–3638. https://doi.org/10.1002/2015GL063946

Press, W. H., Teukolsky, S. A., Vetterling, W. T., & Flannery, B. P. (1996). *Numerical recipes in FORTRAN: The art of scientific computing* (Vol. 1, 2nd ed., pp. 660–664). New York: Cambridge University Press.

Seo, Y., Horwitz, J. L., & Caton, R. (1997). Statistical relationships between high-latitude ionospheric *F* region/topside upflows and their drivers: DE2 observations. *Journal of Geophysical Research*, *102*(A4), 7493–7500.

Strangeway, R. J., Ergun, R. E., Su, Y.-J., Carlson, C. W., & Elphic, R. C. (2005). Factors controlling ionospheric outflow as observed at intermediate altitudes. *Journal of Geophysical Research*, *110*, A03221. https://doi.org/10.1029/2004JA010829

Vasko, I. Y., Agapitov, O. V., Mozer, F. S., Artemyev, A. V., Drake, J. F., & Kuzichev, I. V. (2017). Electron holes in the outer radiation belt: Characteristics and their role in electron energization. *Journal of Geophysical Research: Space Physics*, *122*, 120–135. https://doi.org/10.1002/2016JA023083

Wygant, J. R., Bonnell, J. W., Goetz, K., Ergun, R. E., Mozer, F. S., Bale, S. D., & Tao, J. B. (2013). The Electric Field and Waves instruments on the Radiation Belt Storm Probes mission. *Space Science Reviews*, *179*, 183–220. https://doi.org/10.1007/s11214-013-0013-7

Wygant, J. R., Keiling, A., Cattell, C. A., Johnson, M., Lysak, R. L., Temerin, M., & Spann, J. (2000). Polar spacecraft based comparisons of intense electric fields and Poynting flux near and within the plasma sheet-tail lobe boundary to UVI images: An energy source for the aurora. *Journal of Geophysical Research*, *105*, 18,675–18,692.

Wygant, J. R., Keiling, A., Cattell, C. A., Lysak, R. L., Temerin, M., Mozer, F. S., & Russell, C. T. (2002). Evidence for kinetic Alfvén waves and parallel electron energization at 4–6 R_E altitudes in the plasma sheet boundary layer. *Journal of Geophysical Research*, *107*(A8), SMP 24–1–SMP 24–15. https://doi.org/10.1029/2001JA900113

Zheng, Y., Moore, T. E., Mozer, F. S., Russell, C. T., & Strangeway, R. J. (2005). Polar study of ionospheric ion outflow versus energy input. *Journal of Geophysical Research*, *110*, 7210. https://doi.org/10.1029/2004JA010995